Journal of Molecular Liquids, 33 (1987) 279—310
Elsevier Science Publishers B.V., Amsterdam — Printed in The Netherlands

A NEW AND ORIGINAL PRACTICAL METHOD FOR DETECTING THE SPECTRAL PROPERTIES OF MONOLAYERS OF MOLECULAR MATERIAL ON HOMOGENEOUS AND INHOMOGENEOUS SUBSTRATES

E. HILD[+], M.W. EVANS[++] and G.J. EVANS[*]

+ Research Institute for Telecommunications, Gabor Aron 65, Budapest, Hungary
++ Department of Physics, University College of Swansea, Singleton Park, Swansea SA2 8PP
* Department of Chemistry, University College of Wales, Aberystwyth SY23 1NE

(Received 8 September 1986)

ABSTRACT

A theoretical method is described of using power reflection spectroscopy to detect the spectral properties of layers of molecular material on homogeneous or inhomogeneous solid substrates. Results are presented for non-reflective, partially reflecting and highly reflecting substrates at various angles of incidence in σ and π polarisation. At angles near the Brewster angle of the substrate the nature of the spectrum in pi polarisation is such that a spectral feature due to a surface layer only 1.0 Å thick is visible in the form of a small "blip" on a constant background. For non-metallic and metallic substrates the spectrum is extremely sensitive to the thickness of the liquid layer, polarisation, and angle of incidence, so much so that this method provides a large amount of new information per experiment, much more so than conventional absorption spectroscopy.

INTRODUCTION

The ability to investigate thin layers of molecular material on homogeneous or inhomogeneous substrates is becoming increasingly important in several fields of application. In this paper we illustrate theoretically that under well-defined conditions it is possible to use power reflectivity in pi polarisation to detect layers of molecular liquid on a metallic substrate (e.g. aluminium) approximately 10 Å in thickness. Therefore it is possible, under these conditions, to detect a monolayer of molecular material on a metal substrate. The spectrum is sensitive to polarisation, thickness of surface

0167-7322/87/$03.50

layer, and angle of incidence, so that a reflectivity experiment of this nature provides more useful information than the equivalent power absorption coefficient of traditional spectroscopy, even were this to be possible with layers as thin as 100 Å.

The surface reflectivity of a layered, inhomogeneous, system has been calculated theoretically from the dielectric loss and permittivity of the surface liquid layer using the admittance method, first developed by Jacobsson [1] and later by Hild [2] in a Doctoral Dissertation. The method was applied to inhomogeneous, layered, semiconductor material by Hild and Grofscik [3], and later extended by Hild and Evans [4] to variable angles of incidence. For layered media consisting of liquids superimposed on homogeneous or inhomogeneous substrates a variety of behaviour is encountered in the reflectivity spectra at σ and π polarisation depending on surface liquid thickness, angle of incidence and dielectric nature of the substrates. In this paper the analysis is extended to include an original and new consideration of liquid films on metallic substrates, where again, a variety of behaviour is possible depending on conditions of investigation. These results open up the original possibility of developing a spectroscopy, based on reflectivity from liquids, either resting on a solid substrate, or sandwiched between two windows, the top one transparent over the required frequency ranges and the bottom one a precisely polished aluminium mirror. The film of liquid held between these two windows could be made as thin as practicable, so that the surface properties of mirror layers could be studied as distinct from bulk properties of molecular material. Alternatively, the technique could be used for detecting the presence of monolayers of absorbing liquid or otherwise molecular impurity material on epitaxials of commercial importance [5]. Another possible application would be the study of surface catalysis, and oxide monolayers on metallic material.

THEORETICAL BACKGROUND

Infra-red reflectivity is a popular method of investigating the properties of lightly doped epitaxial layers on heavily doped substrates. There have also been attempts to characterise the diffused or ion-implanted doping profile in semiconductor structures by means of infra-red reflectivity, usually at normal incidence.

The use of arbitrary angles of incidence, as in this work, requires the development of special mathematical methods to solve the Maxwell equations for reflectivity and transmission in non-homogeneous layered media. The

theoretical basis for these methods was worked out initially by Jacobsson [1] and are mentioned in a monograph by Knittl [6]. These methods were arrived at independently by Hild, in a Doctoral Dissertation [2], and were developed considerably by her for use with multi-layer semiconductor systems involving buried layers containing doping profiles. These methods have been described in papers by Hild and Grofscik [3], and have been extended to variable incidence angle by Hild and Evans [4]. For epitaxial semiconductors, this is a considerable improvement on conventional methods which depend on the application of plane-wave formalism. The latter is certainly not the best for solving the second order differential equations - the Maxwell equations - which govern the behaviour of the electromagnetic field vectors in a medium whose optical properties vary, either continuously, or discontinuously.

The methods developed by Hild and co-workers [2-4] enable the calculation of the power reflectance and transmittance of inhomogeneous media by transforming the second order differential equations of the field vectors into first order Riccati type differential equations, which can be integrated using the Runge-Kutta method [4] . Both reflectance and transmittance can be expressed in terms of the optical admittance function. In this section we illustrate additionally how this method can be applied in an original way to monolayers of absorbing material on highly reflecting substrates, either homogeneous or inhomogeneous.

LIGHT PROPAGATION IN INHOMOGENEOUS MEDIA IN TERMS OF THE OPTICAL ADMITTANCE

The electric and magnetic field vectors $\underset{\sim}{E}$ and $\underset{\sim}{H}$ of angular frequency ω obey the following differential equations in an inhomogeneous medium of relative permittivity $\hat{\varepsilon}$ (usually a complex function), and a relative permeability of $\mu = 1$.

$$\Delta\underset{\sim}{E} + \frac{\omega^2}{c^2}\hat{\varepsilon}\,\underset{\sim}{E} - \text{grad div}\,\underset{\sim}{E} = \underset{\sim}{0} \tag{1a}$$

$$\Delta\underset{\sim}{H} + \frac{\omega^2}{c^2}\hat{\varepsilon}\,\underset{\sim}{H} + \frac{1}{\hat{\varepsilon}}\ \text{grad}\,\hat{\varepsilon}\ \text{rot}\,\underset{\sim}{H} = \underset{\sim}{0} \tag{1b}$$

It is assumed that the system is infinite in directions x and y and inhomogeneous only in axis z:

$$\hat{\varepsilon} = \hat{\varepsilon}(z) \tag{2}$$

It is assumed that the interfaces in the system are parallel to plane (x, y),

and that the inhomogeneous layer is on a homogeneous substrate of infinite thickness.

Let a plane wave:

$$A_o = A_o^o \exp(i(\omega t - \underset{\sim}{k}_o^+ . \underset{\sim}{r})) \tag{3}$$

be incident from the air side on the surface of the system at $z = 0$. In equn. (3) "A" denotes any component of the electromagnetic field vectors $\underset{\sim}{E}$ or $\underset{\sim}{H}$, $\underset{\sim}{k}_o^+$ is the wave vector of the incident wave and $\underset{\sim}{r}$ is the position vector.

Assume that k_o^+ lies in the (x,z) plane (the plane of incidence), then:

$$k_x^+ = \frac{\omega}{c} \sin \phi_o; \quad \text{and } k_{oz}^+ = \frac{\omega}{c} \cos \phi_o \tag{4}$$

where ϕ_o is the angle of incidence. The system is homogeneous in direction x, so that the dependence of the field vectors on x can be expressed by the factor:

$$\exp\left(-\frac{i\omega}{c} \sin \phi_o\right) \tag{5}$$

The dependence of the field vector on z will be treated separately for π and σ polarisation. In π polarisation the electric field is parallel to the plane of incidence, and for σ polarisation perpendicular. The σ polarisation corresponds to the transverse electric (TE) mode, with $\underset{\sim}{E}$ in direction y, and the π polarisation to the transverse magnetic (TM) with $\underset{\sim}{H}$ in direction y. The transverse field components Ey and Hy then obey the following differential equations:

$$\frac{\partial^2 Ey}{\partial z^2} + \frac{\omega^2}{c^2} (\hat{\varepsilon} - \sin^2\phi_o) Ey = 0 \tag{6a}$$

$$\frac{\partial}{\partial z} \left(\frac{1}{\hat{\varepsilon}} \frac{\partial Hy}{\partial z}\right) + \frac{\omega^2}{c^2} \left(1 - \frac{\sin^2\phi_o}{\hat{\varepsilon}}\right) Hy = 0 \tag{6b}$$

The parallel and transverse components can be linked with Maxwell's equations:

$$H_x = \frac{1}{i\omega\mu_o\hat{\varepsilon}} \frac{\partial Ey}{\partial z} \tag{7}$$

$$E_x = -\frac{1}{i\omega\varepsilon_o\hat{\varepsilon}} \frac{\partial Hy}{\partial z} \tag{8}$$

where ε_o and μ_o are the permittivity and permeability respectively of vacuum.

OPTICAL ADMITTANCE FUNCTION

This is defined as follows:

$$\hat{j}(z) = -\left(\frac{\mu_o}{\varepsilon_o}\right)^{\frac{1}{2}} \frac{H_t(z)}{E_t(z)} \tag{9}$$

and therefore involves the ratio of the tangential field components H_t and E_t. According to the boundary conditions of Maxwell's equations, H_t and E_t are continuous, so $\hat{j}(z)$ is a continuous function of z in the system unless $E_t = 0$, where the admittance function becomes infinite. The relations between $\hat{j}$ and the transverse field components come from eqn. (9) using eqns (7) and (8):

$$\hat{j}_{TE} = \frac{ic}{\omega} \frac{\partial}{\partial z} (\log_e Ey) \tag{10}$$

$$\therefore \quad Ey = Ey(o)\exp\left(-\frac{i\omega}{c}\int_o^z j(z')dz'\right) \tag{11}$$

by integrating eqn. (10).

Similarly:

$$\gamma_{TM}^{-1} = \frac{c}{i\omega\hat{\varepsilon}} \frac{\partial}{\partial z} (\log_e Hy), \tag{12}$$

$$\therefore \quad Hy = Hy(o)\exp\left(-\frac{i\omega}{c}\int_o^z -\frac{\hat{\varepsilon}(z')}{\hat{j}(z')}dz'\right) \tag{13}$$

Substituting these expressions for Ey and Hy into (6a) and (6b) respectively, we obtain <u>differential equations in the admittance function</u>:

$$\frac{d\hat{j}_{TE}}{dz} = -\frac{i\omega}{c}[\hat{\varepsilon} - \sin^2\phi_o - \hat{j}_{TE}^2] \tag{14}$$

$$\frac{d\hat{j}_{TM}}{dz} = -\frac{i\omega}{c}\left[\left(1 - \frac{\sin^2\phi_o}{\hat{\varepsilon}}\right)\hat{j}_{TM}^2 - \hat{\varepsilon}\right] \tag{15}$$

In the homogeneous parts of the system the field is a combination of a travelling wave with spatial dependence:

$$\exp(-i(k_x x + k_z z)) \tag{16}$$

and of a reflected one with spatial factor:

$$\exp(-i(k_x x - k_z z)) \tag{17}$$

where

$$k_x = \frac{\omega}{c} \sin \phi_o \tag{18}$$

$$k_z = \frac{\omega}{c} [\hat{\epsilon}_h - \sin^2\phi]^{\frac{1}{2}} \tag{19}$$

The optical admittance of the travelling wave in a homogeneous medium is therefore:

$$\begin{aligned} \hat{j}_{h,TE} &= \frac{c}{\omega} \hat{k}_z = (\hat{\epsilon}_h - \sin^2\phi_o)^{\frac{1}{2}} \\ \hat{j}_{h,TM} &= -\frac{\hat{\epsilon}\omega}{c\hat{k}_z} = \frac{\hat{\epsilon}_h}{(\hat{\epsilon}_h - \sin^2\phi_o)^{\frac{1}{2}}} \end{aligned} \tag{20}$$

Eqn. (20) defines the wave admittance and it is denoted by $\hat{\eta}$. Therefore:

$$\hat{j}_h = \hat{\eta} \tag{21}$$

for the travelling wave, and:

$$\hat{j}_h = -\hat{\eta} \tag{22}$$

for the reflected one. There is only a single travelling wave in the homogeneous, seminfinite, substrate, so:

$$\hat{j}_s(z) = \hat{\eta}_s \qquad \text{for } z \geq z_s, \tag{23a}$$

and because of the continuity of j:

$$\hat{j}(z_s) = \hat{\eta}_s \tag{23b}$$

serves as a boundary condition for the differential equations (14) and (15), the Ricatti type eqns. for the optical admittance.

The field in the medium from which the light beam has emerged is the sum of the incident and reflected wave:

$$\underset{\sim}{E}_o = \underset{\sim}{E}_o^+ + \underset{\sim}{E}_o^- , \tag{24}$$

$$\underset{\sim}{H}_o = \underset{\sim}{H}_o^+ + \underset{\sim}{H}_o^- \tag{25}$$

The reflection coefficients can now be defined as the ratio of the transverse components of the field vectors in the reflected wave to those in the incident wave:

$$r_{TE} = \frac{E^-_{oy}(o)}{E^+_{oy}(o)} \; ; \quad r_{TM} = \frac{H^-_{oy}(o)}{H^+_{oy}(o)} \tag{26}$$

There is a direct connection between the reflection coefficients and the optical admittance. For the TE mode:

$$\gamma(o) = \left(\frac{\mu_o}{\varepsilon_o}\right)^{\frac{1}{2}} \frac{H_x(o)}{E_y(o)} = -\left(\frac{\mu_o}{\varepsilon_o}\right)^{\frac{1}{2}} \frac{H^+_{ox} + H^-_{ox}(o)}{E^+_{oy}(o) + E^-_{oy}(o)}$$

$$= -\left(\frac{\mu_o}{\varepsilon_o}\right)^{\frac{1}{2}} \frac{H^+_{ox}(o)/E^+_{oy}(o) + \hat{r}_{TE} H^-_{ox}(o)/E^-_{oy}(o)}{1 + \hat{r}_{TE}}$$

$$= \hat{\eta}_{TE} \left(\frac{1 - \hat{r}_{TE}}{1 + \hat{r}_{TE}} \right) \tag{27}$$

The same formula can be derived for the TM mode so the reflection coefficients in both modes can be obtained from the surface value of the corresponding optical admittance:

$$\hat{r} = \frac{\hat{\eta}_o - \hat{j}(o)}{\hat{\eta}_o + \hat{j}(o)} \; . \tag{28}$$

The power reflectance is then:

$$R = |r|^2 \tag{29}$$

With eqn. (28) it is possible to calculate the reflectance of a system of arbitrary $\hat{\varepsilon}(z)$ in the range $0 \leq z \leq z_s$ if one knows the optical admittance at z_s and solves the differential equations (9) of $\hat{j}$ at $z = 0$.

Expressions for the transmittance can also be derived in terms of $\hat{j}$. Assume that the system is bounded by the same medium (air) on both sides. By definition the transmission coefficients are:

$$\hat{t}_{TE} = \frac{E^+_{sy}(z_s)}{E^+_{oy}(o)} \; ; \quad \hat{t}_{TM} = \frac{H^+_{sy}(z_s)}{H^+_{oy}(o)} \; ; \tag{30}$$

Because of the continuity of the y components of the field vectors and because of eqns. (14) and (15):

$$E^{+}_{sy}(z_s) = E_y(z_s) = E_y(o)\exp\left(- \frac{i\omega}{c} \int_o^{z_s} \hat{j}(z')dz' \right) \tag{31}$$

where the subscript refers to the medium and the electric field in the inhomogeneous layer is denoted by Ey. We have seen that:

$$Ey(o) = E^{+}_{oy} + E^{-}_{oy} = E^{+}_{o}(1 + \hat{r}_{TE}) \tag{32}$$

so:

$$\hat{t}_{TE} = (1 + \hat{r}_{TE})\exp\left(- \frac{i\omega}{c} \int_o^{z_s} \hat{j}(z')dz' \right) \tag{33}$$

and, in the same way,

$$\hat{t}_{TM} = (1 - \hat{r}_{TM}) \exp\left(\frac{i\omega}{c} \int_o^{z_s} \hat{\varepsilon}(z')\hat{j}^{-1}(z')dz' \right) \tag{34}$$

The power transmittance is defined as:

$$T = |\hat{t}|^2 \tag{35}$$

If there is a homogeneous layer in the system with boundaries z_{h1} and z_{h2} the field in this layer is again a combination of a travelling wave and a reflected one.

$$\hat{j}_h = \hat{\eta}_h \, [1 - 2/ \, [1-\hat{p}^{-1}\exp(^2 \, \frac{i\omega}{c}\left(\varepsilon_h - \sin^2\phi_o \right)^{\frac{1}{2}}\Delta z)]] \tag{36}$$

where

$$\hat{\rho} = (\hat{\eta}_h - \hat{j}(z_{h2}))/(\hat{\eta}_h + \hat{j}(z_{h2})) \tag{37}$$

is the reflection coefficient at the "back" boundary of the homogeneous layer, and:

$$\Delta z = z_{h2} - z_{h1} \quad ; \quad z_{h2} \geq z \geq z_{h1} \tag{38}$$

For numerical calculations it is more convenient to use real variables and to use the wavenumber ($\bar{\nu}$) instead of ω. Let us introduce the real variables through the formulae.

$$\hat{j} = j_1 - ij_2 \quad ; \quad \eta = \eta_1 - i\eta_2 \quad ;$$

$$\hat{\varepsilon} = \varepsilon_1 - i\varepsilon_2 \tag{39}$$

$$\hat{\varepsilon}_s = \varepsilon_{s1} - i\varepsilon_{s2}$$

$$\hat{\eta}_s = \sqrt{\hat{\varepsilon}_s} = \eta_s - ik_s \ .$$

The algorithm to calculate the reflectance of an inhomogeneous layer on a homogeneous substrate of refractive index n_s and absorption index k_s consists of solving the system of the first order differential equations:

$$\frac{dj_1}{dz} = 2\pi\bar{\nu}\ (-\varepsilon_2 + 2j_1j_2) \tag{40a}$$

$$\frac{dj_2}{dz} = 2\pi\bar{\nu}(\varepsilon_1 - \sin^2\phi_o - j_1^2 - j_2^2) \tag{40b}$$

for the TE mode, and

$$\frac{dj_1}{dz} = 2\pi\bar{\nu}[\varepsilon_2 - 2j_1j_2 + \frac{\sin^2\phi_o}{\varepsilon_1^2+\varepsilon_2^2}\ [2\varepsilon_1j_1j_2 - \varepsilon_2(j_1^2 + j_2^2)]] \tag{41a}$$

$$\frac{dj_2}{dz} = 2\pi\bar{\nu}[\varepsilon_1 - j_1^2 + j_2^2 + \frac{\sin^2\phi_o}{\varepsilon_1^2+\varepsilon_2^2}\ [\varepsilon_1(j_1^2 - j_2^2) + 2\varepsilon_2j_1j_2]] \tag{41b}$$

for the TM mode, with the boundary conditions:

$$j_1(z_s) = \eta_{s1} \ ; \quad j_2(z_s) = \eta_{s2} \tag{42}$$

where η_{s1} and η_{s2} are the real and imaginary parts respectively, of the wave admittance of the substrate.

The reflectivity is obtained by the following formulae:

$$R = \frac{(\eta_o - j_1(o))^2 + j_2(o)^2}{(\eta_o + j_1(o))^2 + j_2(o)^2} \tag{43}$$

where $\eta_o = \cos\phi_o$ for the TE mode and

$\eta_o = -1/\cos\phi_o$ for the TM mode

and η_{s1} and η_{s2} are calculated as follows

Let:

$$\tilde{\varepsilon}_1 = \varepsilon_{s1} - \sin^2\phi_o; \quad \tilde{\varepsilon}_2 = \varepsilon_{s2} ;$$

$$y_1 = [0.5(\varepsilon_1 + E)]^{\frac{1}{2}} \quad ; \quad y_2 = 0.5[E - \tilde{\varepsilon}_1]^{\frac{1}{2}} ,$$

then $\eta_{s1} = y$; $\eta_{s2} = y_2$ for the TE mode, and

$$\eta_{s1} = \frac{-\varepsilon_{s1}y_1 - \varepsilon_{s2}y_2}{E} \quad ; \quad \eta_{s2} = \frac{-\varepsilon_{s2}y_1 + \varepsilon_{s1}y_2}{E}$$

for the TM mode.

RESULTS AND DISCUSSION

In this section we consider reflectivity from a surface liquid layer on different types of substrates. The dielectric loss and permittivity of the liquid are both governed by a simple theory based on the truncation of the Mori linear continued fraction expansion of the orientational autocorrelation function, fully described elsewhere in the literature [7].

The three variable Mori theory used to produce the infra red absorption is an approximation to the Lioville equation which governs the dynamics of an ensemble of N molecules in the liquid state. It defines the dielectric loss and permittivity (ε'' and ε' respectively) as follows [7].

$$\varepsilon''(\omega) = \frac{(\varepsilon_o-\varepsilon_\infty)\gamma\phi_o(o)\phi_1(o)}{\gamma^2(\phi_o(o)-\omega^2)^2 + \omega^2(\omega^2-(\phi_o(o) + \phi_1(o)))^2} \tag{44}$$

$$\varepsilon'(\omega) = \varepsilon_o-(\varepsilon_o-\varepsilon_\infty)\omega^2 \frac{\gamma^2(\omega^2-\phi_o(o))+(\omega^2-\phi_1(o))(\omega^2-(\phi_o(o)+\phi_1(o)))}{\gamma^2(\phi_o(o)-\omega^2)^2+\omega^2(\omega^2-(\phi_o(o)+\phi_1(o)))^2} \tag{45}$$

Where ε_o is the static permittivity and ε_∞ that at the end of the high frequency of the absorption process (at about 200 cm^{-1}). The far infra-red power absorption coefficient in terms of the dielectric loss and permittivity is then, as usual:

$$\alpha(\bar{\nu}) = \frac{2\sqrt{2}\pi\varepsilon''(\bar{\nu})\bar{\nu}}{[(\varepsilon'(\bar{\nu}) + \varepsilon''(\bar{\nu})^2)^{\frac{1}{2}} + \varepsilon'(\bar{\nu})]^{\frac{1}{2}}} \tag{46}$$

where the wavenumber is $\bar{\nu} = \omega/(2\pi c)$.

The effective Debye relaxation time in this theory is

$$\tau_D = \frac{(\phi_o(o) + \phi_1(o))^2 - 2\phi_o(o)\gamma^2}{\phi_o^2(o)\gamma^2} \qquad (47)$$

The parameters ϕ_o,ϕ_1 and γ govern the shape of the far infra red spectrum and can also be defined in terms of molecular and inter molecular properties. $\phi_o(o)$ is related to the root mean square molecular angular velocity; $\phi_1(o)$ to the mean square torque; and γ to the Debye relaxation time through eqn (47). Therefore ϕ_o is defined through the geometry of the molecular and the equipartition theorem in the usual way; but ϕ_1 needs for its definition a knowledge of the intermolecular mean square torque. Usually the latter can be obtained from a computer simulation. The results in fig. (1) are for

$$\gamma = 1.0 \times 10^{13}\ \text{sec}^{-1}\ ;\quad \phi_o(o) = 1.0 \times 10^{25}\ \text{sec}^{-1};$$

$$\phi_1(o) = 1.0 \times 10^{25}\ \text{sec}^{-1}.$$

This gives a relatively sharp peak in ε'' and a dispersion for ε' which includes a negative portion. Transformed with eqn (47) into power absorption this would provide a sharp far infra red peak, usually observable in liquid crystals.

It is important to note that the theory leading to fig. (1) is used in this paper only for the sake of illustration. In general any type of infra red absorption can be used as a basis for generating reflectivity using the new admittance method of this paper, including experimental data from any sample (e.g. a low dimensional deposition on a solid super lattice).

Whenever the infra red peak (or peaks) is (or are) sharp, the equivalent dielectric dispersion can become negative before reaching the final plateau at the positive value of ε_∞. This means that the dispersion cuts the abscissa at a certain wavenumber $\bar{\nu}_o$ on the high frequency side of the loss peak. It

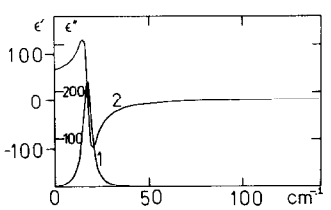

Fig. 1. The basic loss (1) and dielectric permittivity (2) used to generate the power reflectivity curves of this paper.
Ordinate: Permittivity; Asscissa: wavenumber/cm^{-1}

will be shown in this section that this property leads to an additional feature in the reflectivity at pi polarisation at the frequency $\bar{\nu}_o$. The shape and contrast of this feature are strongly dependent on polarisation, angle of incidence and the thickness of the surface layer. There would be several such features if the absorption spectrum of the thin surface layer consisted of several sharp peaks, as is usually the case at liquid helium temperatures in low dimensional materials of interest.

In the theory used for the sake of illustration in this section the width of the loss peak in fig. (1) and therefore the depth of the negative trough in the dispersion, is controlled essentially by the ratio ϕ_1/γ. The greater this ratio the sharper the loss, and therefore the sharper the power absorption. This means that the sharper the loss peak the more clearly discernible will be the new reflectivity feature at $\bar{\nu}_o$ illustrated in this section. This could be most useful analytically for the study of infra red reflectivity from low dimensional materials. In a spectrum of natural (i.e. experimentally observed) infra red frequencies there would be plenty of scope to see the pi reflectivity in the infra red provided conditions are optimised.

The absorption equation from the loss (eqn (44)) and the dispersion (eqn (45)) is too complex for analytical integration when used in the fundamental equations (14) and (15) but the Runge Kutta integrator used in the algoirthm behind this work is easily accurate enough to overcome this difficulty, and for homogeneous substrates is very fast. The effect on the spectrum of varying the ratio ϕ_1/γ for a given ϕ_o can be investigated straightforwardly. The algorithm could also be adapted to compute reflectivity spectra from a set of experimental absorption data suitably parameterised.

i) Assuming that the substrate is pure silicon, it can be represented in dielectric terms by a constant permittivity $\varepsilon_o = 11.7$ and zero dielectric loss [3,4].

ii) A polished metallic substrate is a nearly perfect reflector, and can be represented [8] by a very high constant dielectric loss ε'' and a much lower dielectric permittivity because the pure metal becomes transparent to radiation well above the infra-red range in which we are interested. In this work, we also chose to use a highly reflecting substrate with a constant permittivity: i) of 1,000 and ii) 10,000 and zero loss throughout the frequency range of interest.

RESULTS FOR SILICON SUBSTRATE [3,4]

The dielectric loss and permittivity of the surface liquid layer is shown in Fig. (1) for illustration. The reflectivity coefficients computed in π and σ polarisation in the figures that follow are all based on the same dielectric properties for the surface liquid layer - those of Fig. (1). These figures attempt to illustrate the wide range of information available from R_σ and R_π as a function of a) surface liquid thickness; b) angle of incidence; c) polarisation of the probe radiation, for the same sample. This information can be stored in the data-base of a computer and used as a very detailed fingerprint of the optical properties of the sample under investigation.

The first series of figures in this section deals with a surface liquid layer of 1.0×10^{-4} cm on a substrate of permittivity $\varepsilon_o = 11.7$ (silicon), for various angles of incidence - (ϕ). It can be seen from Fig. 2(a) that as the incidence angle departs from the normal ($\phi = 20^o$), the R_σ and R_π power reflection coefficients are already significantly different from those for $\phi = 0^o$. In particular, for π polarisation, a second inverted peak is visible in Fig. 2(a) at 76 cm^{-1}, the point at which the dielectric permittivity in Fig. (1) cuts the frequency axis for the second time.

As the angle is increased to 61.874^o the R_σ and R_π curves become distinctly separated (Fig. 2(b)) the feature at pi polarisation at 76 cm^{-1} , the point at which the dielectric permittivity in Fig. (1) cuts the frequency axis for the second time.

As the angle is increased to 61.874^o the R_σ and R_π curves become distinctly separated (Fig. 2(b)) the feature at pi polarisation at 76 cm^{-1} now shows signs of being a dispersion, Fig. 2(c) showing clearly that it is in the process of "inverting" from a negative to a positive peak. It is interesting to note in this context that an angle of incidence of 61.874^o corresponds to $\tan^{-1}(\varepsilon_{\infty,liq}^{\frac{1}{2}})$, where $\varepsilon_{\infty,liq}$ is the high frequency limit of the dielectric permittivity of the liquid, and this compares with the spectrum at $\phi = 73.701^o$ in Fig. 2(c) which is the Brewster angle [4,9] of the substrate, $\tan^{-1}\varepsilon_\infty^{\frac{1}{2}} = \tan^{-1} 11.7^{\frac{1}{2}}$. It is significant that in π polarisation at the Brewster angle of $\phi = 73.701^o$ (Fig. 2(c)), the higher frequency peak has become the greater in magnitude, and is the most visible feature in the landscape.

As the incidence angle is increased to 85^o (Fig. 2(d)) there is yet another interesting development in the spectrum at pi polarisation, in that

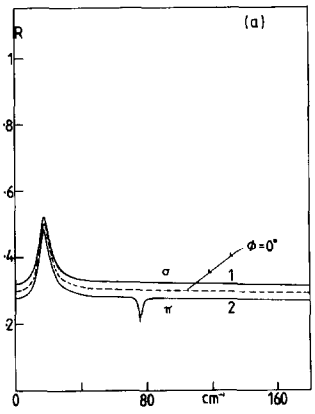
(a)
R
1
·8
·6
·4
·2
σ
Φ=0°
1
π
2
0
80
cm⁻¹
160

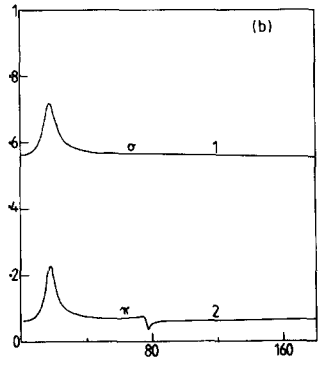
(b)
1
·8
·6
·4
·2
0
σ
1
π
2
80
160

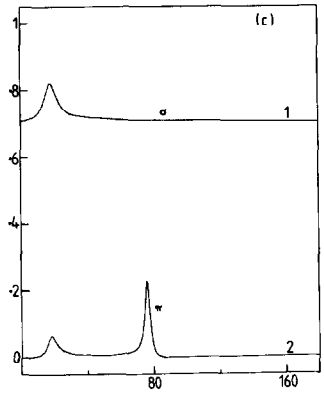
(c)
1
·8
·6
·4
·2
0
σ
1
π
2
80
160

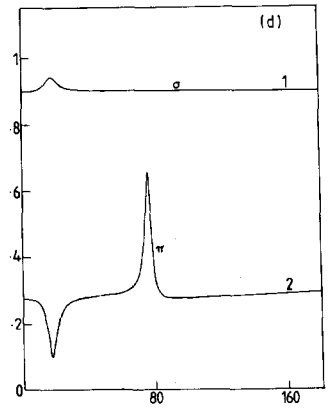
(d)
1
·8
·6
·4
·2
0
σ
1
π
2
80
160

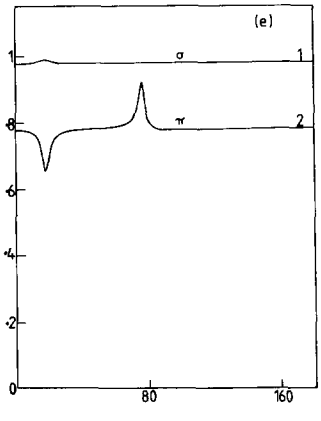
(e)
1
·8
·6
·4
·2
0
σ
1
π
2
80
160

the higher frequency peak continues to grow, but the lower frequency peak now inverts and becomes negative. Therefore the "peak pattern" in Fig. 2(d) is the mirror image of that in Fig. 2(a), the lower frequency peak has inverted from positive to negative and the higher frequency peak from negative to positive. Finally, at a glancing angle of 89^{o} the power reflectivity spectra in both polarisations converge to the constant value of unity expected when the beam is precisely parallel to the surface of the reflector.

The series of spectra 2(a) to 2(e) therefore contain a great deal more information than the simple loss and dispersion curves of Fig. (1) from which they are all derived, using admittance theory. Reflection spectroscopy, when used in this way, therefore provides a completely original and much more detailed fingerprint than a conventional infra-red absorption spectrum. This is especially true of molecular liquids.

When the thickness of the surface liquid layer is increased to 0.1 mm (Fig. 3)) the corresponding change in the reflectivity spectra, both in σ and π polarisation, is pronounced (cf. Fig. (2) and Fig. (3)). In particular, the peak at low frequency in Fig. (2) has evolved into a triplet of fringes which are deeper in π polarisation compared with those in σ polarisation at incidence angles of 61.874^{o}, 73.701^{o} and a glancing angle of 89^{o} (Fig. 3(c)). The higher frequency feature in Fig. (2) has evolved in Fig. (3) into a sharp "band edge", followed at higher frequency by a set of fringes, which are considerably deeper in σ than in π polarisation, at 61.874^{o}, the angle defined by $\tan^{-1} \varepsilon_{\infty,liq}^{\frac{1}{2}} = \tan^{-1} 3.5^{\frac{1}{2}}$. If this angle is increased further to $73.701^{o} = \tan^{-1} \varepsilon_{\infty,sub}^{\frac{1}{2}} = \tan^{-1} 11.7^{\frac{1}{2}}$ (the Brewster angle [4,9] of the silicon substrate), then the R_{σ} and R_{π} signals become separated on the ordinate scale, the R_{σ} signal being so far the more reflective. The low frequency triplet pattern and higher frequency "band edge" are followed at this angle by a set of very deep interference fringes, which are again more pronounced in sigma polarisation than in pi. Finally, at the glacing angle

---

Fig. 2. Surface liquid layer of 1.0×10^{-4} cm on a substrate of permittivity $\varepsilon_{o} = 11.7$, and no dielectric loss.

a) Incidence angle of $\phi = 0$ (- - - -); and $\phi = 20^{o}$: (1) in σ polarisation; (2) in π polarisation.

b) Incidence angle of $\phi = 61.874^{o}$, (1)σ polarisation; (2)π polarisation. Ordinate: Power Reflectivity; Absciasa: cm^{-1}

c) As for b), $= \tan^{-1} 11.7^{\frac{1}{2}} = 73.701^{o}$ (Brewster angle).

d) As for b), $= 85^{o}$, note the inversion in the low frequency peak for angles greater than the Brewster angle.

e) As for b), $\phi = 89^{o}$, a "glancing" angle.

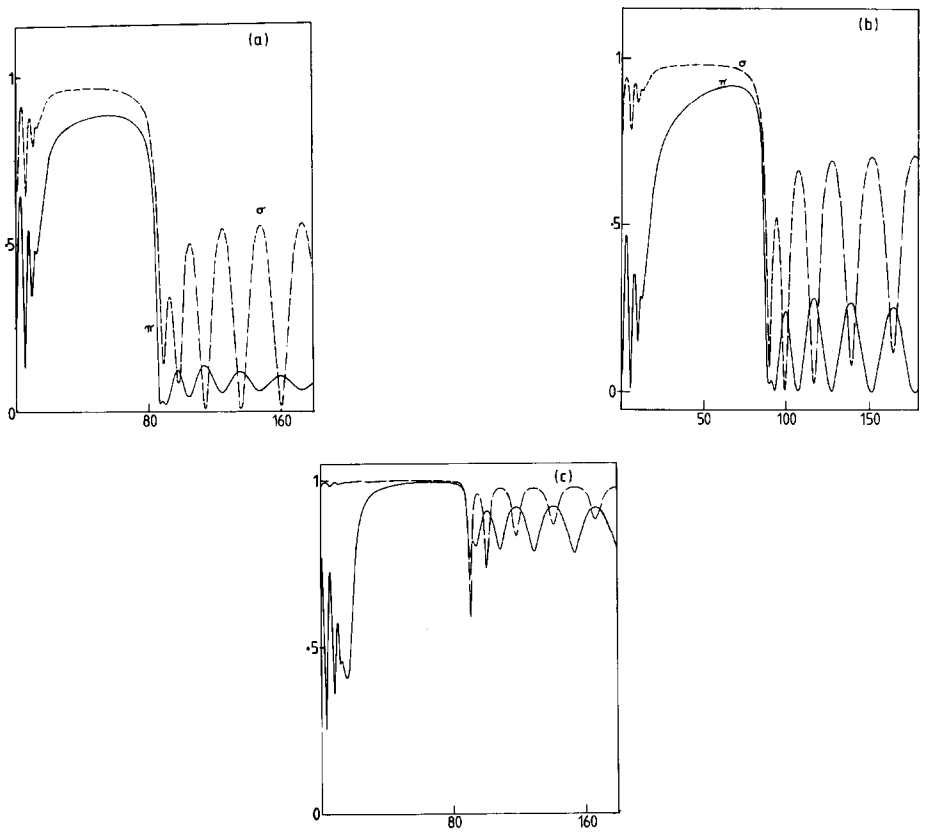

Fig. 3. As for Fig. (2), surface liquid layer of 1.0×10^{-2} cm (= 0.1 mm).
a) - - - - - -σ polarisation; _____ π polarisation; $\phi = 61.874^{o}$.
b) $\phi = 73.701^{o}$; c) $\phi = 89^{o}$.

of 89^{o} the patterns of R_{σ} and R_{π} have again changed significantly in particular the triplet in R_{π} at low frequency has evolved into a slightly more complex pattern with four peaks. Both spectra, in R_{σ} and R_{π} are converging to the value of unity at all $\bar{\nu}$ for $\phi = 90^{o}$. Therefore, the patterns in Fig. (2) and (3) provide detailed fingerprint information on the properties of liquid surface layers as a function of incidence angle and liquid depth.

HIGHLY REFLECTING SUBSTRATES [8]

This section provides theoretical results for a surface liquid layer on highly reflecting substrates. These results are obtained from the dielectric

loss and permittivity of Fig. (1) and aim to demonstrate the detection by power reflection spectroscopy of very thin layers of molecular liquid placed on a highly reflective substrate. This entirely original technique could be useful in detecting monolayers of surface material and in studying by reflectivity low dimensional materials [6] arranged on highly reflecting substrates such as front polished aluminium mirrors.

Two different types of reflecting substrates are considered.

i) Substrate material with a very high, constant, permittivity in the far infra-red range, and no dielectric loss.

ii) Metallic substrates, typified by pure aluminium, whose optical properties in the far infra-red have recently been determined experimentally [8] . From this work it is possible to see that the dielectric loss of Al in the far infra-red is approximately constant to about 200 cm^{-1}, and is about 320,000. The dielectric permittivity of aluminium on the other hand is small in this region [8] . We have estimated a value of about 1.5 from the work in the literature [8]. The reflectivity at normal incidence of Al in the far infra-red is about 0.997 - a value taken from the same literature source.

1. SUBSTRATE OF VERY HIGH CONSTANT PERMITTIVITY

For a liquid layer of 1.0×10^{-4}cm the spectrum takes on the appearance of a very sharp spike (Fig. 4(a)) centred in π polarisation at a frequency (76 cm^{-1}) corresponding to that at which the permittivity dispersion in Fig. (1) cuts the abscissa from negative to positive at high frequency. In Fig. 4(a) the dielectric permittivity of the substrate is ε_o = 1,000 and the dielectric loss is zero. As the angle of incidence increases from $\phi = 40^o$ to $\phi = 61.874^o$ the high frequency R_π spike becomes deeper and would be easy to discern if the reflectivity technique were to be used for the investigation of surface liquid layers on reflecting substrates of this nature. Another useful feature of this type of spectroscopy is revealed when the angle of incidence is increased to near glancing. The first signs of this change are discernible at $\phi = 85^o$, where the high frequency peak has inverted with respect to that for $\phi = 61.874^o$ in Fig. 4(b). In the region between 85^o and 90^o the R_σ spectrum is featureless near 1.00, but the R_π spectrum becomes extremely sensitive to small changes in incidence angle (Fig. 4(d)) and therefore provides a useful fingerprint of the properties of the surface liquid layer. At the Brewster angle defined by $\tan^{-1} 1000^{\frac{1}{2}} = 88.189^o$ (Fig. 4(d)) the R_π dependence has changed out of all recognition from that of Fig. 4(a) or 4(b). A further

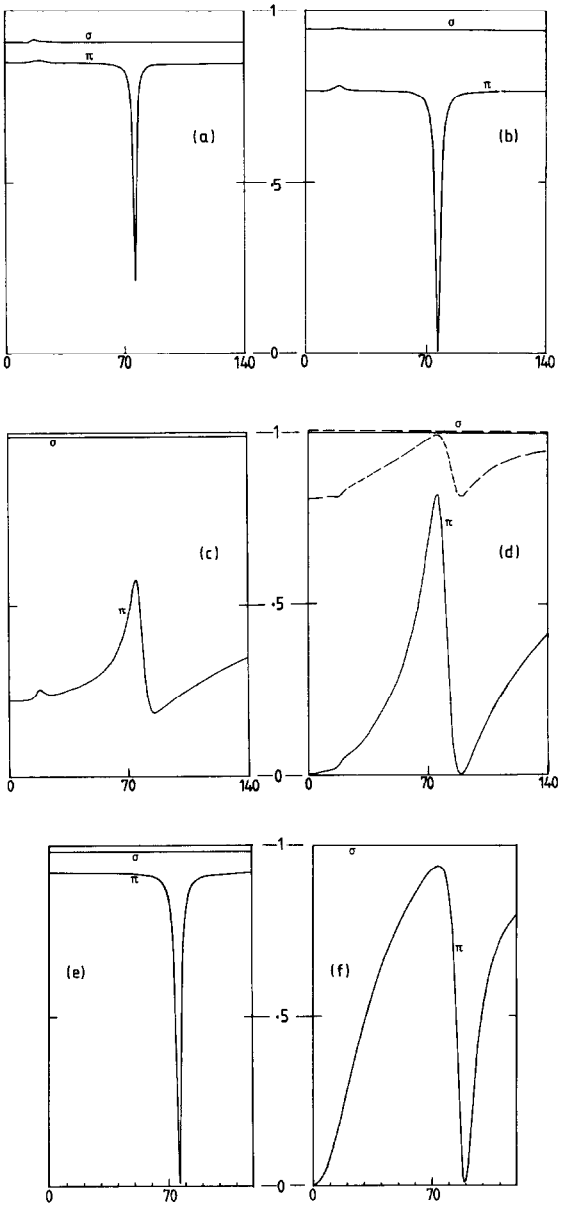

Fig. 4. Surface liquid layer of 1.0×10^{-4} cm on a substrate of high, constant, permittivity, $\varepsilon_o = 1{,}000$. (1)σ polarisation; (2)π polarisation.
a)$\phi = 40^o$; b)$\phi = 61.874^o$; c)$\phi = 85^o$; d)$\phi = 89.9^o$; e) $\varepsilon_o = 10{,}000, \phi = 61.874^o$; f) $\varepsilon_o = 10{,}000, \phi = 89.427^o$.

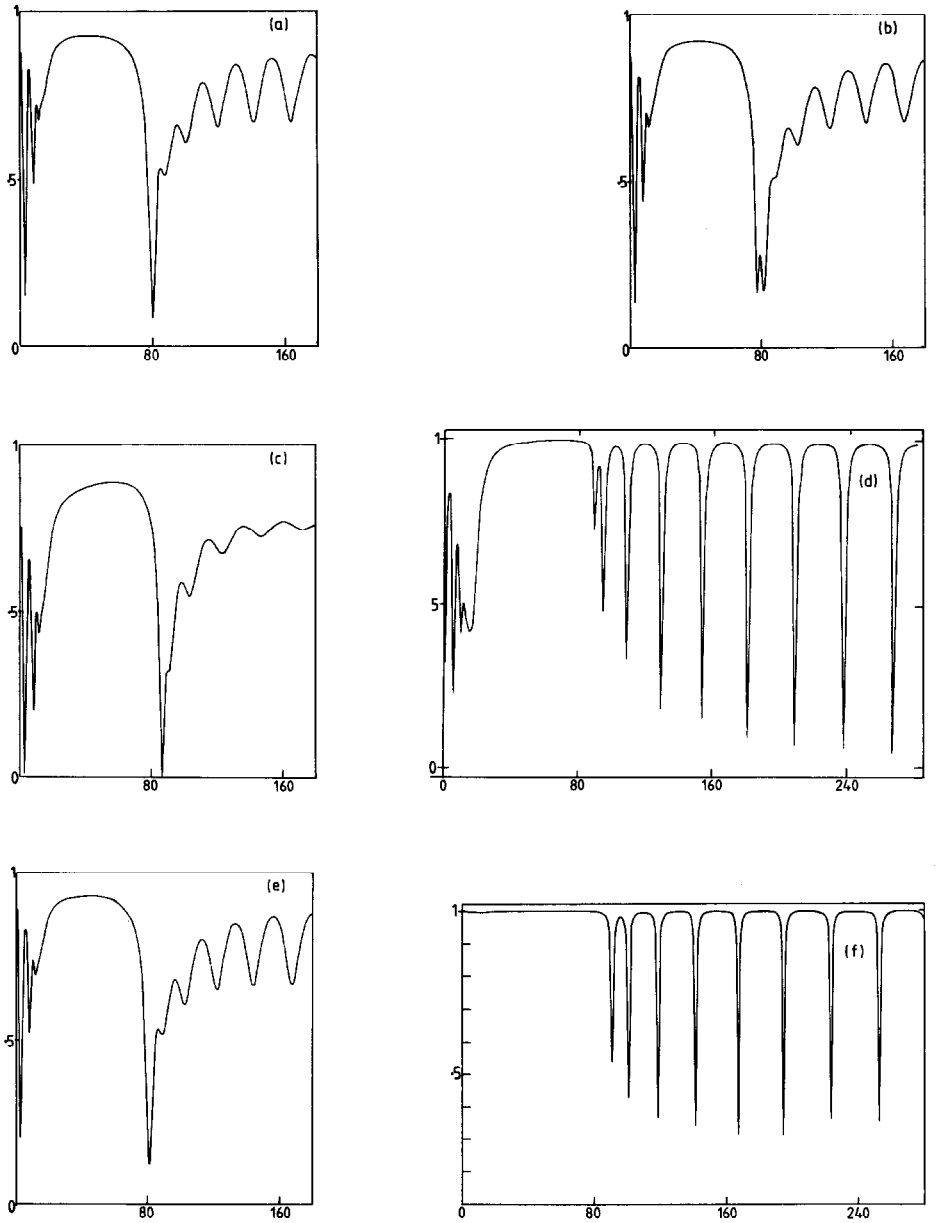

Fig. 5. Surface layer of 0.1 mm on a substrate of constant permittivity $\varepsilon_o = 1000$; R_π. a) $\phi = 0^o$; b) $\phi = 20^o$; c) $\phi = 61.874^o$; d) $\phi = 89^o$ e) $R_\sigma, \phi = 20^o$; f) $R_\sigma, \phi = 89^o$.

increase of this angle to 89.9° (Fig. 4(d)) means that the whole R_π profile is shifted up the complex ordinate scale and approaches the limiting value of unity expected at 90°. If the permittivity of the substrate is increased to 10,000, again for zero loss, Fig. 4(e) and 4(f) show that the pattern is repeated as ϕ is increased from 61.874° to the Brewster angle of $\tan^{-1} 10{,}000^{\frac{1}{2}} = 89.427°$.

For a substrate $\varepsilon = 1000$, and a surface liquid layer of 0.1 mm the R_π spectra computed from Fig. (1) are shown in Fig. (5). In the sequence (5a) to 5(d) the R_π spectrum is shown as the incidence angle is increased from $\phi = 0°$ (normal to $\phi = 89°$ (Fig. 5(d)). The most obvious change in the spectrum

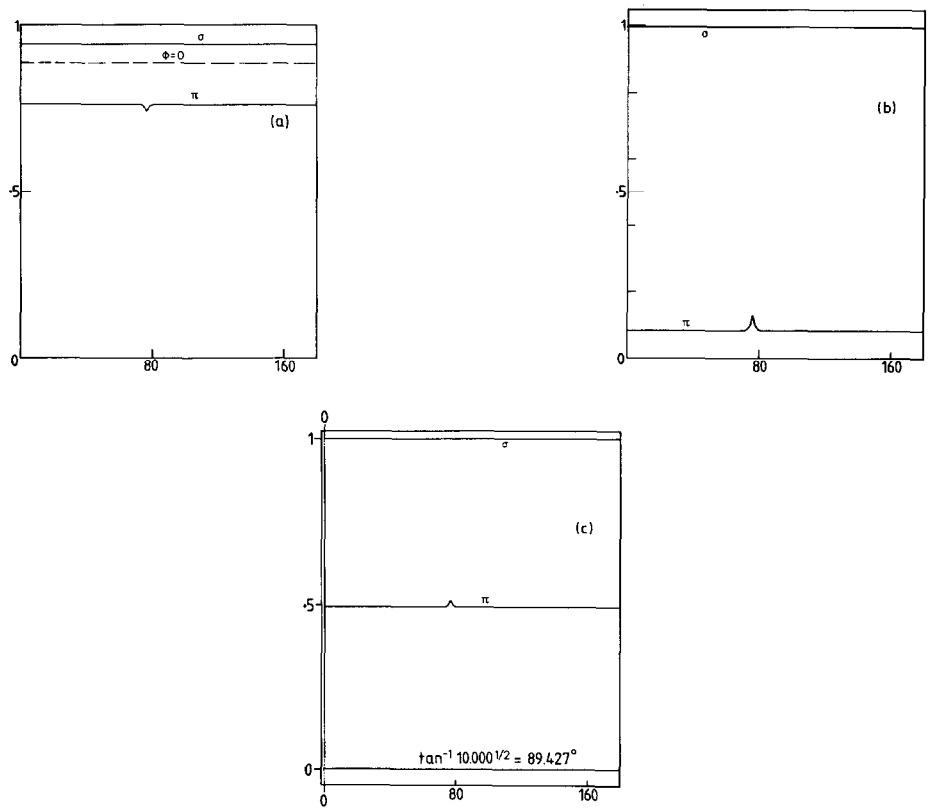

Fig. 6. Surface layer of 100 Å on a substrate of constant permittivity $\varepsilon_o = 1000$; (1) R_σ; (2) R_π.
a) $\phi = 61.864°$, - - - - - - $\phi = 0$; (b) $\phi = 89°$; (c) $\phi = 89.9°$.

is that for angles greater than the Brewster angle ($\phi = 88.189^{o}$) the high frequency interference fringes become sharp and pronounced (Fig. (5d)). The sharp inverted peak at 80 cm^{-1} is split in various ways as the angle is increased, and the triplet feature at low frequencies is inverted as ϕ becomes greater than 88.189^{o}. Note that these features are all generated self-consistently from the simple loss and dispersion curves of Fig. (1). This pattern is echoed in sigma polarisation (Figs. 5(e) and 5(f)), but the lower frequency features at $\phi = 89^{o}$ in R_{σ} have vanished.

For surface liquid layers of 100 Å and 10 Å depth the R_{π} and R_{σ} spectra (Fig. 6)) are changed markedly from those of Fig. (5). At $\phi = 61.864^{o}$ a small peak at 76 cm^{-1} in π polarisation is clearly visible in Fig. 6(a) on a substrate of permittivity $\varepsilon = 1000$. In Fig. 6(b), it is clear that increasing the angle to $\phi = 89^{o}$ results in the inversion of this peak from negative to positive. In Fig. 6(c) of this series the R_{π} peak at 89.9^{o} is clearly visible for a 10 Å depth of surface liquid on a substrate of permittivity 10,000. This implies that the technique of power reflectivity should be useful for the detailed study of monolayers [6] of absorbing material on a highly reflecting substrate.

Finally, in Fig. (7) it is demonstrated that the nature of the substrate has an effect on the surface reflectivity, even at normal incidence. This illustration is for a surface liquid layer of depth 1.0×10^{-4} cm on a substrate composed of a transition layer of 1.0×10^{-4} cm on an infinite bottom layer of permittivity 1.5.

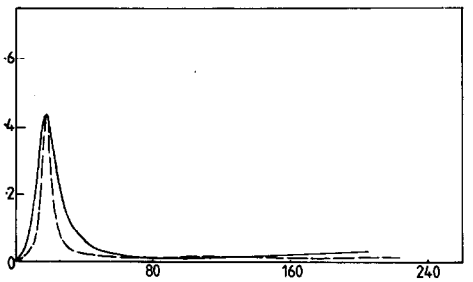

Fig. 7. Illustration of inhomogeneity of substrate on surface reflectivity.
_____ σ polarisation
- - - - π polarisation.

RESULTS FOR A SURFACE LIQUID LAYER ON ALUMINIUM SUBSTRATE

The optical properties of metallic aluminium have recently been investigated thoroughly [8] from the far infra-red to the ultra-violet, and it can be estimated that the permittivity of metallic aluminium up to about 200 cm^{-1} is approximately constant at about 1.5, and that the dielectric loss is approximately constant at about 320,000 up to approximately 200 cm^{-1}. These values were used in our program to calculate the power reflectivity from surface liquid layer on metallic aluminium e.g. a front polished aluminium mirror. The Brewster angle in this case is determined by the dielectric loss, and is:

$$\phi_B = \tan^{-1} 320{,}000^{\frac{1}{2}} = 89.8987^{\circ}.$$

There the R_π spectrum changes shape at an angle a few minutes of arc above the parallel. It is shown in this section that low angle reflectivity of this nature in pi polarisation is able, theoretically, to detect and characterise a layer of liquid on the substrate only 1.0 Å (1.0×10^{-8} cm) thick. This new and original method could therefore be of great practical interest in the optical investigation of low dimensional materials, monolayers, and interfaces between materials.

As the depth of the surface liquid layer decreases it becomes clear that the conventional technique of normal incidence reflectivity will lose all spectral information, both in R_σ and R_π. Information is retained in R_π only, and is available in proliferation at low angles of incidence, to an arc minute ± fifty or so arc seconds above the parallel. The practical means of setting up an optical apparatus to observe these R_π spectra should be based on the methods already in use [10] for low angle X-ray scattering. It will be necessary to use precisely collimated tunable laser radiation 100% polarised into sigma or pi. The reflected laser beam will be analysed by a spectrometer, either an interferometer or using conventional prisms or gratings, depending on the frequencies of interest (i.e. far infra-red, infra-red, visible, ultra-violet, or perhaps microwave and radio frequency).

ILLUSTRATIVE RESULTS

These are given for the dielectric loss and permittivity of Fig. (1) and for various depths of surface liquid layer and angle of incidence ϕ.

In Fig. (8) the depth is 0.1 mm (10^{-2} cm). At this depth, and for an

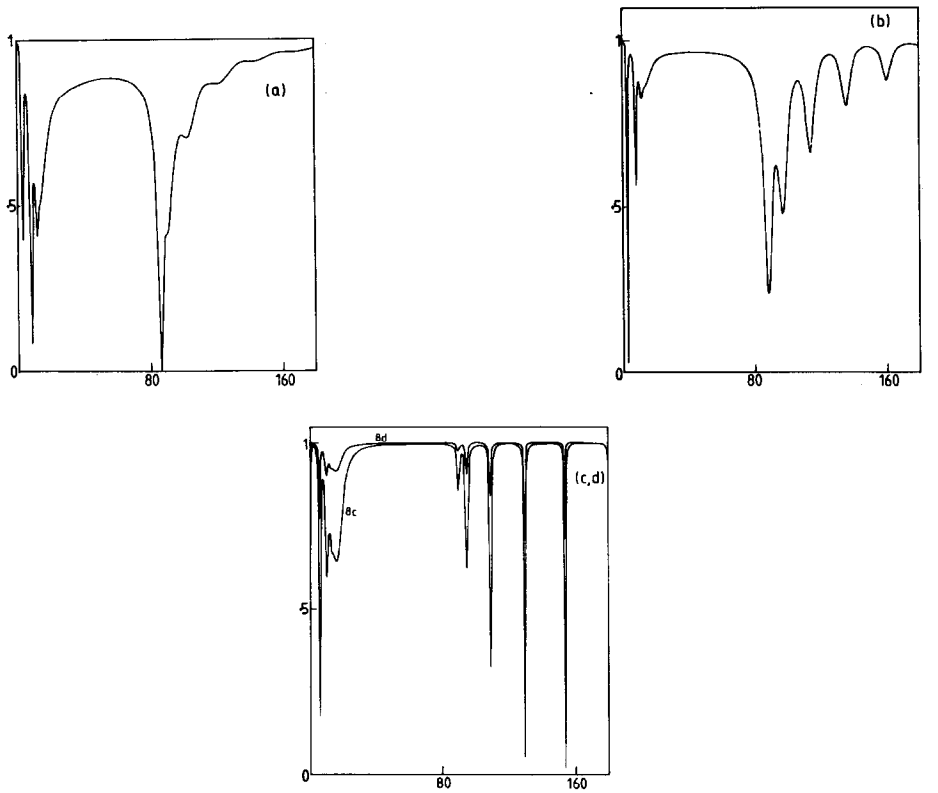

Fig. 8. Reflectivity on an aluminium substrate. Surface liquid depth = 1.0×10^{-2} cm.

a) R_π at $\phi = 61.874^o$;

b) R_σ at $\phi = 61.874^o$;

c) R_π at $\phi = 89.500^o$ and d) R_π at $= 89.8987^o$

angle of incidence of 61.874^o detailed fingerprints are observable both in R_σ (Fig. 8(a)) and in R_π (Fig. 8(b)). The R_σ and R_π spectra cover the full scale from 1.0 to 0.0, giving plenty of opportunity for spectral analysis of the surface liquid layer. For $\phi = 89.500^o$, just below the Brewster angle (Fig. 8(c)), the R_π spectrum has "inverted" at low frequencies and the high frequency, full scale, fringes have sharpened and are well defined. In R_σ polarisation (not shown), the reflectivity at low frequency, in great contrast, is dominated completely at this angle by that of aluminium [8] (0.997). Nothing is therefore observable in R_σ except some residual high frequency

fringes, which appear in a different frequency pattern, however, to those illustrated in Fig. 8(c) at R_π.

At the Brewster angle of $\phi = 89.8987^o$ (Fig. 8(d)) the R_π spectrum has shifted up-scale, and is approaching the value of $R_\pi = 1.000$ for all $\bar{\nu}$ expected at $\phi = 90.0000^o$, when the radiation does not, of course, enter the sample, being precisely parallel to the surface of the liquid. For this depth of liquid layer the spectrum does not change dramatically in shape near the Brewster angle, but the fringes are "dampened" from full scale (Fig. 8(c)) to about quarter scale for about 30 arc minutes change in angle. The amplitude of the spectrum is therefore extremely sensitive to angle of incidence near the parallel.

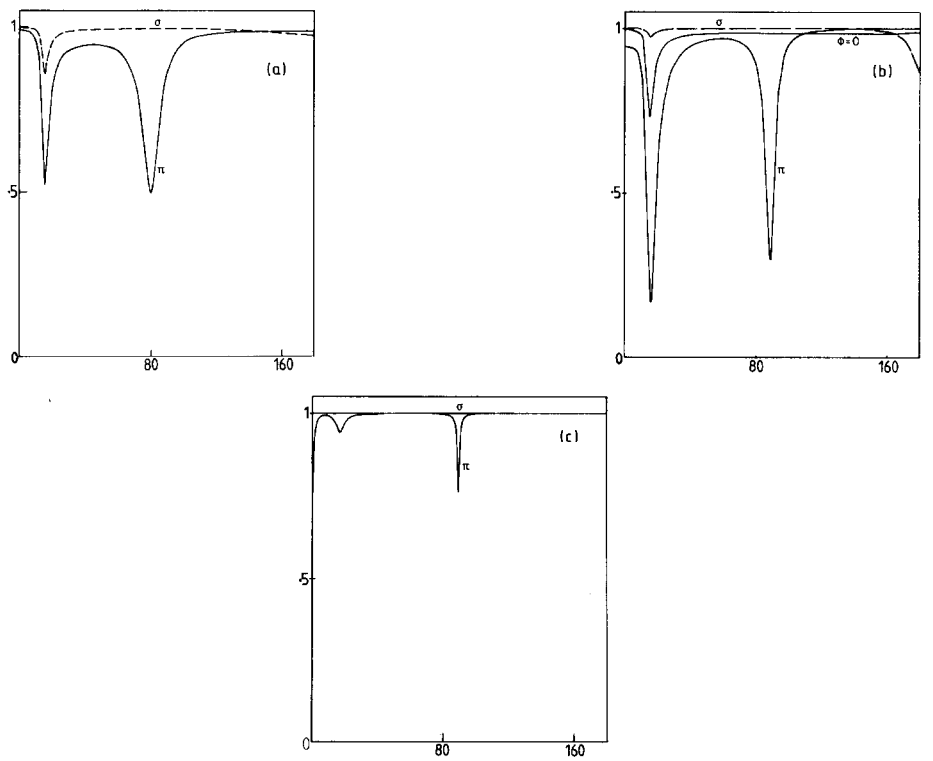

Fig. 9. As for Fig. (8). Surface depth = 1.0×10^{-3} cm.

a) - - - - R_σ; _____ R_π at $\phi = 61.874^o$

b) (1) - - - - - R_σ; _____ R_π at = 85.000^o

(2) - - - - - $R_\sigma = R_\pi$ at $\phi = 0^o$

c) _____ (1) R_σ; _____ (2) R_π at $\phi = 89.8987^o$.

For a surface liquid depth of 100,000 Å (10^{-3} cm) the reflectivity spectra are completely different in appearance (Fig. 9) from those of Fig. (8). At $\phi = 61.874^{o}$ (Fig. 9(a)) there are no interference fringes visible, because they have become widely separated in frequency by reducing the liquid depth from 10^{-2} cm to 10^{-3} cm. The R_{σ} and R_{π} profiles in Fig. 9(a) consist of one inverted peak (R_{σ}) and two for R_{π}. The minima of the R_{π} peaks correspond exactly with the frequency in Fig. (1) of the maximum of the dielectric loss (17.5 cm^{-1}) and the frequency (78.0 cm^{-1}) where the permittivity cuts the abscissa for the second time, negative to positive.

Fig. 9(b) contrasts the R_{σ} and R_{π} profiles at $\phi = 0$ (normal incidence) and $\phi = 85^{o}$ (low angle of incidence). At $\phi = 0$, $R_{\sigma} = R_{\pi}$, and the reflectivity consists of one inverted peak at 17.5 cm^{-1}. At $\phi = 85^{o}$, in great contrast, the R_{σ} profile is dominated by the aluminium substrate [8], and the 17.5 cm^{-1} feature is barely visible. In R_{π} two features are clearly visible, at 17.5 cm^{-1} and 76 cm^{-1}, and are almost full scale. Therefore it would be much more useful to study the R_{π} profile at $\phi = 85.000^{o}$. Finally for this depth (100,000 Å) Fig. 9(c) illustrates R_{σ} and R_{π} at the Brewster angle $\phi = 89.8987^{o}$. The R_{π} profile has shifted upscale, as in Fig. 8(d), but now there is visible in Fig. 9(c) a clear change of shape in R_{π}, because there has appeared around zero frequency a new "spike". Therefore the R_{π} spectrum now consists of three clear features, but the R_{σ} spectrum, in great contrast, is simply a constant very close to 1.000 for all $\bar{\nu}$, and tells us nothing at all.

For a surface depth of liquid of 10,000 Å (10^{-4} cm) the spectra, both in R_{σ} and R_{π}, become dominated at sub-Brewster angles by a sharp, full-scale, spike at 76 cm^{-1}. For example, Fig. (10a), at $\phi = 50.7685^{o}$, where the original loss peak-frequency at 17.5 cm^{-1} is invisible on the scale of the diagram. Note that nothing at all is visible in R_{σ}, except the (approximately) constant reflectivity [8] of the aluminium substrate (0.997). In R_{π} however, the profile is dominated entirely by the full-scale feature at 76 cm^{-1}. At normal incidence ($\phi = 0$) this 76 cm^{-1} spike vanishes completely, so that this illustrates the information lost by conventional normal-incidence, reflectivity. In this case it loses everything that is there to observe. As the angle is increased to $\phi = 85^{o}$ (Fig. 10(b)), the 76 cm^{-1} (R_{π}) feature of Fig. (10(a)) broadens and flattens to half-scale, and the original 17.5 cm^{-1} feature becomes just visible as a shallow, broad trough. Also the main spike in Fig. 10(b) has shifted up-frequency to 78 cm^{-1}. However, as the incidence angle ϕ is increased to the Brewster angle (Fig. 10(c)) there is a great change in the appearance of the spectrum in R_{π}. The high frequency spike again becomes much sharper and to full-scale, but is shifted to 89 cm^{-1}. Additionally a

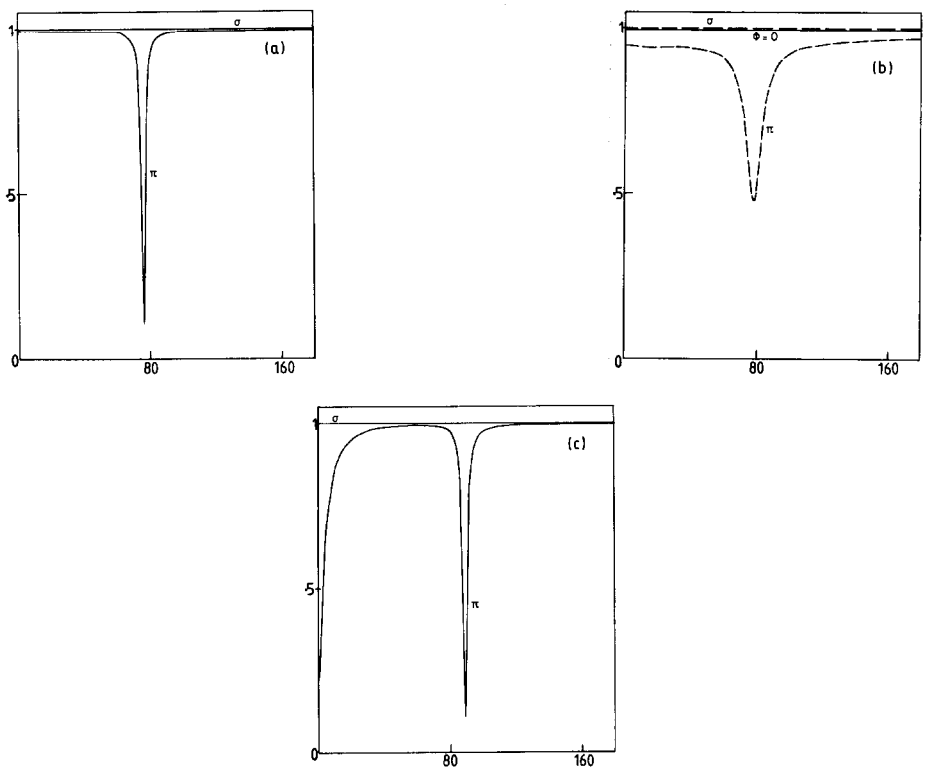

Fig. 10. As for Fig. (8), surface liquid depth = 1.0×10^{-4} cm.
a)_____ (1) R_σ; _____(2) R_π at $\phi = 50.7685^o$.
b) - - - - (1) R_σ; - - - - (2) R_π at $\phi = 85.000^o$.
3) _____$R_\sigma = R_\pi$ at $\phi = 0^o$
c) _____(1) R_σ; _____ (2) R_π at $\phi = 89.8987^o$.

pronounced zero frequency spike changes the whole aspect of things at low frequency, the original 17.5 cm^{-1} feature having completely disappeared. The R_σ profile (Fig. 10(c)) in contrast is simply total reflection for all $\bar{\nu}$.

Comparing Figs (9) and (10) it is clear that the underlying pattern is similar, but that this is emphasized quite differently for 10,000 Å (Fig. 10)) as opposed to 100,000 Å (Fig. (9)), i.e. Fig. (10) is a variation on the theme of Fig. (9). The "fingerprints" for the two cases are quite distinct and easily recognisable. Note that all these various patterns are generated mathematically, and therefore entirely consistently, from the one simple loss peak [7] of Fig. (1).

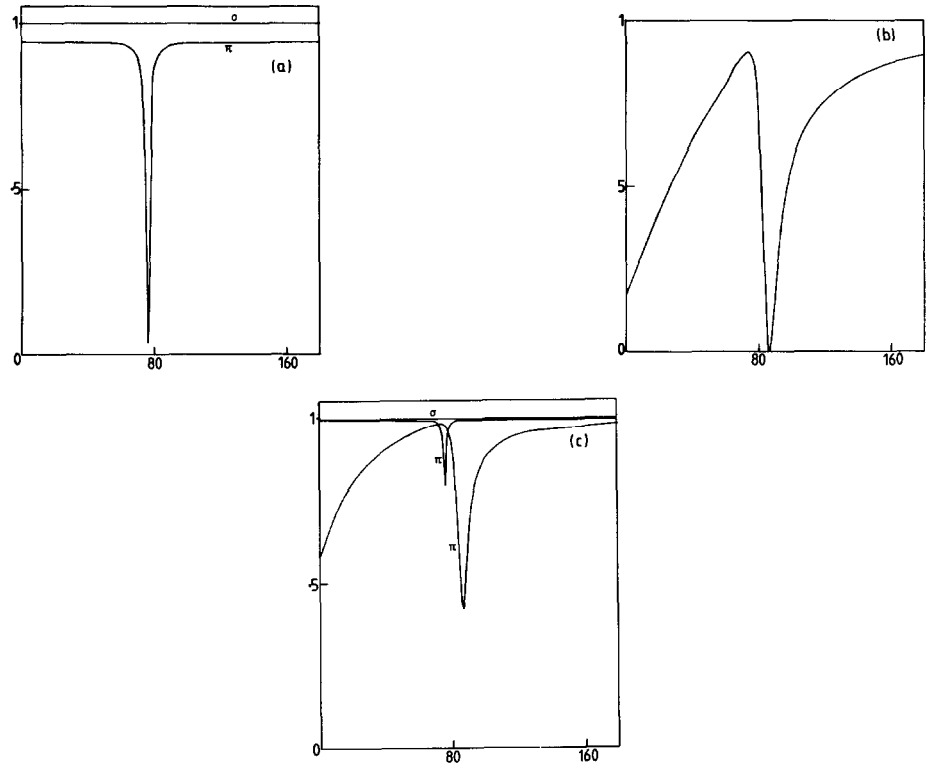

Fig. 11 As for Fig. (8), surface liquid depth = 1.0×10^{-5} cm.

a) _____(1) R_σ; _____(2) R_π; at $\phi = 85.000^\circ$

b) _____(1) R_σ; _____(2) R_π; at $\phi = 89.8987^\circ$.

c) _____(1) R_π at $\phi = 50.7685^\circ$

_____ (2) R_π at $\phi = 89.980^\circ$

_____ (3) R_σ at both angles.

The equivalent patterns for a surface liquid depth of 1,000 Å (10^{-5} cm) (Fig. (11)) are developments of those in Fig. (10). A layer of 1,000 Å is about 200 small molecules thick, and it is therefore of practical importance to note for $\phi = 85^\circ$ (Fig. 11(a)) that the 76 cm^{-1} spike is full-scale. This implies that it would be straightforward to observe the spectral properties of a 1,000 Å depth of liquid in R_π. Additionally the pi spectrum from $\phi = 85^\circ$ to the Brewster angle (Fig. 11(b)) is dramatically sensitive to a small change of 4.8987°. At $\phi_B = 89.8987^\circ$ the zero frequency feature, which first became visible in Fig. (9(c)), has come to dominate the R_π profile,

and the full scale high frequency minimum of Fig. 11(a) has shifted to 86 cm^{-1}. This gives ample scope to study the R_π properties of a 1,000 Å surface layer in practice. In Fig. 11(c) the R_π profiles are contrasted at $\phi = 50.7685^o$ and $\phi = 89.980^o$, and it is clear that the use of low angles amplifies considerably, the small spike observable at 76 cm^{-1} at $\phi = 50.7685^o$. The R_π profile at $\phi = 89.980^o$ (about one arc minute from the parallel) shows that above the Brewster angle the R_π spectrum retains the overall profile at the Brewster angle itself (Fig. 11(b)), but shifts very rapidly up-scale to the value of $R_\pi = 1.000$ for all $\bar{\nu}$ which it must attain, from simple physical considerations, at $\phi = 90.000^o$. This change, for aluminium substrate, must occur in just over 0.1^o (six arc minutes) so that the R_π spectrum must, accordingly, be extremely sensitive to a six arc minute variation in incidence angle. Again, this gives plenty of scope for precise practical investigation of an entirely original kind.

SURFACE LIQUID LAYERS OF 100 Å (10^{-6} cm) AND LESS

In this limit there is room only for about twenty small molecules, on rough average, from the surface of the liquid to the surface of the aluminium. Several other limits are being reached simultaneously, some technical, some theoretical. For example:

i) The molecular dynamics of the surface liquid layer may no longer be those of a bulk liquid, if, say, 100,000 Å. The vibrational, rotational, and translational motions of the molecules may be affected by frequent collisions with the surface of the aluminium, so that classical or quantum statistical mechanics of bulk liquids [7] do not apply.

ii) Practical considerations. For example it may not be possible to obtain a surface liquid layer of 100 Å or less without the use of a top window to trap the layer on the aluminium substrate. However, it is possible to develop the theory described in this article for reflectivity from a window, liquid, aluminium system. Naturally, the surface of the aluminium substrate must be machined and polished to high precision when dealing with angstroms of surface layer. However, if the latter is not a liquid but a solid low dimensional material (monolayer) of some type, then what follows proves that R_π Brewster angle reflectivity can be used to detect, theoretically, surface layers of down to 1.0 Å (10^{-8} cm) on aluminium substrate over the whole range of the electromagnetic spectrum.

Taking the loss peak and dispersion of Fig. (1) for a theoretical 100 Å layer of liquid (10^{-6} cm), the dependence of R_π on ϕ is illustrated in Fig. (12).

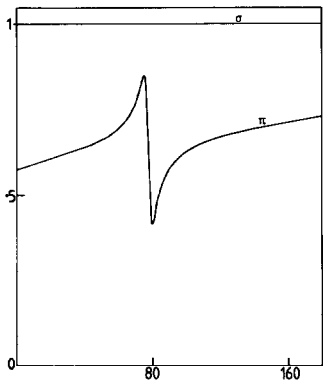

Fig. 12. As for Fig. (8), surface liquid depth = 1.0×10^{-6} cm.

The pattern of Fig. (11) is accentuated, and the original sharp zero frequency feature which made its first appearance in Fig. 9(c) has broadened across the whole spectrum in Fig. (12), which is in the process of transition to one composed of a feature centred around 76 cm^{-1} superimposed on a fairly constant R_π background, the level of which is determined by the incidence angle ϕ. At around the Brewster angle in Fig. (12) there is the now familiar sensitivity, of R_π on ϕ, both in shape and amplitude, so that a 100 Å layer, if one could be prepared, is quite easy to characterise. Note that R_σ gives no information at all now, it is, to within 10^{-5}, unity for all ϕ and $\bar{\nu}$.

Assuming that the technology becomes available to prepare a surface film of molecular material of 10 Å, with the dielectric properties of Fig. (1), on an aluminium mirror polished to a tolerance of an angstrom or less, the dependence of R_π on ϕ is that of Fig. (13). This figure concentrates on an arc of a few minutes either side of $\phi_B = 89.8987^o$ because at higher incident angles the 76 cm^{-1} feature is less visible. At $\phi = 89.500^o$ (30 minutes of arc from the parallel) the spike at 76 cm^{-1} covers a range of about 0.1 in R_π, and this is easily enough for its practical observation. A further useful feature is the sensitivity of the R_π background to ϕ. In Fig. 13(a), R_π at $\phi = 85.000^o$ is at 0.94, but is at 0.57 at 89.500^o. The 76 cm^{-1} spike is much less visible, however, at $\phi = 85.000^o$, and the position of the original loss peak of Fig. (1), at 17.5 cm^{-1} is completely undiscernible for all ϕ. At the Brewster angle (Fig. 13(b)), the background R_π is down to 0.175 ± 0.005, and the signature of the 76 cm^{-1} feature is starting to change into "first-differential", i.e. a positive peak followed immediately by a negative peak.

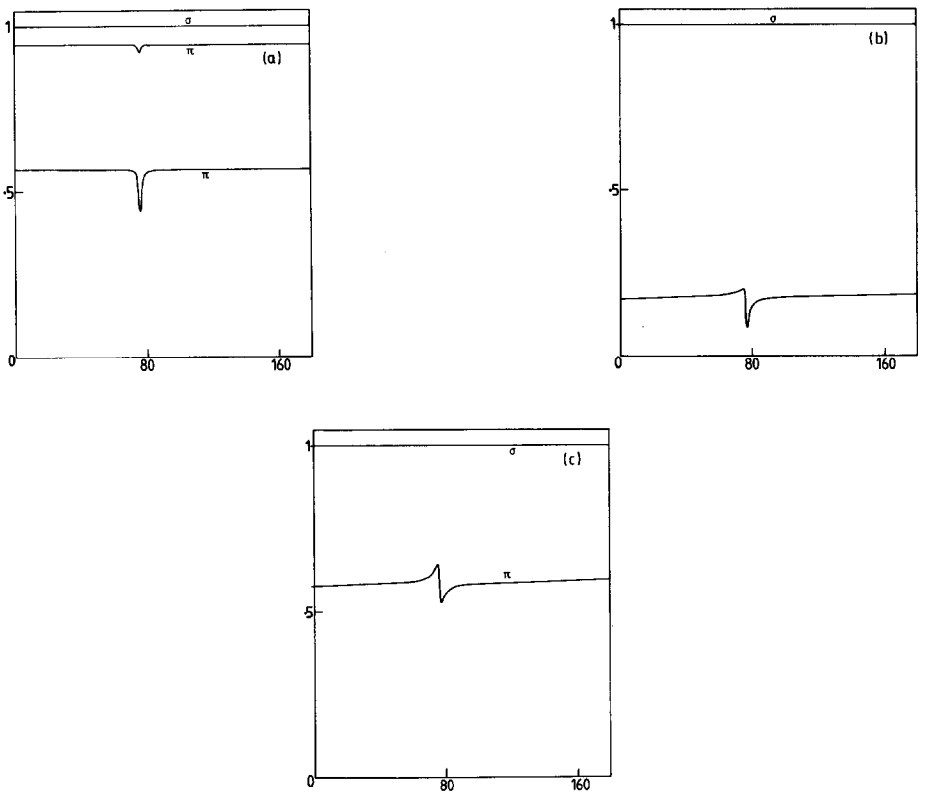

Fig. 13. As for Fig. (8), surface liquid depth = 1.0×10^{-7} cm.
a) _____(1) R_π at $\phi = 89.500^o$; _____(2) R_π at $\phi = 85.000^o$; _____(3) R_σ for both angles.
b) _____(1) R_σ; _____(2) R_π; at $\phi = 89.900^o$.
c) As for (b), $\phi = 89.8987^o$.

This process is complete at $\phi = 89.980^o$ (Fig. 13(c)), and the background has moved up scale to about 0.58 ± 0.005.

For a 10 Å surface liquid depth R_σ is unity (to within 10^{-8}) for all ϕ and $\bar{\nu}$.

Finally, Fig. (14) shows that it is possible, theoretically, to characterise a surface film only 1.0 Å (10^{-8} cm) in thickness. Fig. (14a) illustrates the change in signature as we sweep through the Brewster angle from $\phi = 89.500^o$ to $\phi = 89.980^o$. The result at the Brewster angle itself is shown in Fig. (14(b)) and shows the considerable fall in background level.

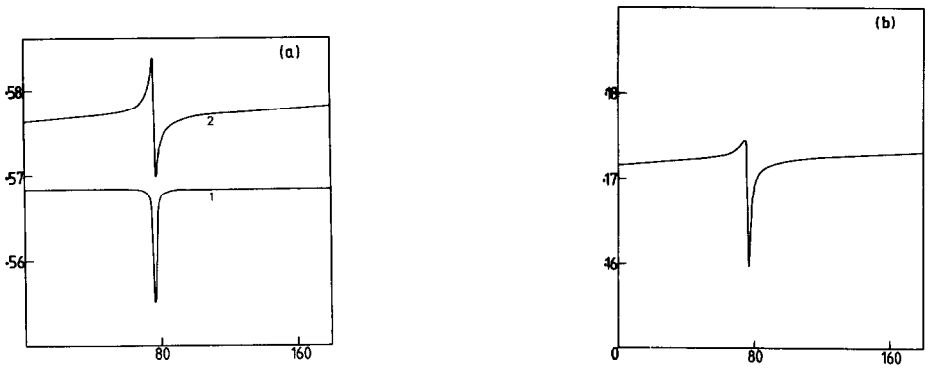

Fig. 14 As for Fig. (8), surface liquid depth = 1.0×10^{-8} cm.
a) _____(1) R_π at $\phi = 89.500^o$
_____(2) R_π at $\phi = 89.980^o$
b) R_π at $\phi = 89.900^o$.

CONCLUSIONS

1. The theoretical R_σ and R_π spectra in Figs. (2) to (14) have all been generated, using admittance theory, from the simple far infra-red peak of Fig. (1), using different solid substrates, angles of incidence, and surface thicknesses.
2. These theoretical results show in great detail that the use of reflectivity, especially at angles near the Brewster angle in pi polarisation, will be of practical importance in the infra-red study of low dimensional materials, monolayers, interfaces between layers, and similar constructs.

ACKNOWLEDGEMENTS

This work was supported by the Nuffield Foundation, the Leverhulme Trust, S.E.R.C. and the University of Wales.

REFERENCES

1 R. Jacobsson, "Light Reflection from Films of Continuously Varying Refractive Index", in Progress in Optics, Vol. 5 (1965).
2 E. Hild, Doctoral Dissertation, Technical University of Budapest, (1976).

3 E. Hild and A. Grofcsik, Infra-red Physics., 18 (1978) 23.

4 E. Hild and M.W. Evans, J. Applied Phys., 59 (1986) 1822.

5 B. Senitzky and S.P. Weeks, J. Applied Phys., 52 (1981) 5308.

6 Z. Knittl, "Optics of Thin Films", Wiley-Interscience, New York, London (1976).

7 M.W. Evans, G.J. Evans, W.T. Coffey and P. Grigolini, "Molecular Dynamics" (Wiley/Interscience, New York, 1982), chapters 1 to 3.

8 E. Shiles, T. Sasaki, M. Inokut and D.Y. Smith, Phys. Rev. B., 22 (1980) 1612.

9 M.W. Evans, J. Chem. Soc., Faraday Trans. II, 76 (1980), 1147.

10 S.E.R.C. Daresbury Laboratory, Annual Reports.